Stereodynamics in reaction $O(^1D) + CH_4 \rightarrow OH + CH_3$*

Sha Guang-Yan(沙广燕)[a], Yuan Jiu-Chuang(袁久闯)[b], Meng Chang-Gong(孟长功)[a]†, and Chen Mao-Du(陈茂笃)[b]‡

[a] *School of Chemistry, Experimental Center of Chemistry, Dalian University of Technology, Dalian* 116024, *China*

[b] *School of Physics and Optoelectronic Technology, and College of Advanced Science and Technology, Dalian University of Technology, Dalian* 116024, *China*

(Received 22 May 2013; revised manuscript received 8 June 2013; published 3 December 2013)

A theoretical study of the stereodynamics for reaction $O(^1D) + CH_4 \rightarrow OH + CH_3$ has been carried out using the quasiclassical trajectory method (QCT) on a potential energy surface structured by Gonzalez *et al*. The integral cross sections (ICSs), differential cross sections (DCSs) and product rotational angular momentum polarization have been calculated. With the collision energy increasing, the ICS decreases. There is no threshold energy, because no barrier is found on the minimum energy path. The DCS results show that the backward and forward scatterings exist at the same time. With the collision energy increasing, the dominant rotation of the product changes from the right-handed direction to the left-handed direction in planes parallel to the scattering plane. In the isotopic effect study, the decrease of the mass factor weakens the polarization degree of the rotational angular momentum vectors of the products.

Keywords: quasiclassical trajectory method, product polarization, isotope effect

PACS: 82.30.Cf, 82.20.Fd, 82.20.Kh **DOI:** 10.1088/1674-1056/23/1/018202

1. Introduction

In the atmosphere, methane is the most abundant hydrocarbon and one of the most important atmospheric species. Following the ultraviolet (UV) photo dissociation of ozone, the first electronically excited state of atomic oxygen forms; this process is an important initiator of the free radical chemistry.[1] The reaction of $O(^1D) + CH_4 \rightarrow OH + CH_3$ is an important source of OH in the dry stratosphere.

The dynamic study of the atom plus diatom reaction has had great development in both theoretical and experimental research, where the breadth and depth have reached a high extent. The dynamic study of the polyatomic reaction is at the primary stage due to its complexity. However, the polyatomic reaction has attracted more and more attention with the development of the experimental technique and computer technology. Within the last decade, some studies have been carried out on the polyatomic reaction of $O(^1D) + CH_4$ and its isotopic reaction.[1–24] On the experimental side, the universal crossed molecular beam apparatus is used to investigated the reaction $O(^1D) + CH_4$.[2–4] Miller *et al.* used the ultrafast, time-resolved and state-resolved experiments to investigate the mechanism of the title reaction.[5] The crossed molecular beam technique with sliced velocity map imagine was used by Shuai *et al*. to investigate the isotopic reaction of $O(^1D) + CD_4 \rightarrow OD + CD_3$ and remarkably different features were found in the forward and backward scatterings.[6] On the theoretical side, Gonzalez and Hernando presented two ground state potential energy surfaces of the title reaction using the second and the fourth order Moller–Plesset methods with a large basis set, where the potential energy surfaces (PESs) were used to study the reaction dynamics.[7–9] Chang *et al*. calculated the rate constants of CH_3OH dissociation and the statistical branching ratios for various product channels by the Rice–Ramsperger–Kassel–Marcus (RRKM) theory and the vibrational RRKM theory based on their *ab initio* potential energy surface.[10,11] Yu *et al.* calculated the stationary point geometries and frequencies on the lowest singlet potential energy surface for the CH_3OH system using the complete-active-space self-consistent-field method.[12]

Most of the previous works on the title reaction focused on the scalar properties, such as the rate constant and the product population distribution. However, to understand the overall mechanism of the reaction, the study of scalar is not enough; only by mastering the scalar and vector properties together can we get the whole picture of the scattering dynamics. In the early years, some important works about the vector properties of a gas-phase reaction were done by Fano and Macek, Herschbach *et al*.[25–28]; after this, the study of vector properties on the gas-phase reaction gets a great development in both experiment and theory.[29] In this work, we pay more attention to the vector properties of the title reaction. This paper is organized as follows. The theoretical method is briefly reviewed in Section 2. The results and discussion are presented in Section 3. Finally, Section 4 provides a conclusion.

*Project supported by the National Natural Science Foundation of China (Grant Nos. 21271037 and 10974023).

†Corresponding author. E-mail: cgmeng@dlut.edu.cn

‡Corresponding author. E-mail: mdchen@dlut.edu.cn

© 2014 Chinese Physical Society and IOP Publishing Ltd

2. Theory

2.1. Triatomic model potential energy surface

In this paper, the triatomic model is applied to reduce the amount of computation. In the model, the CH_3 group is treated as a pseudo atom, so the reaction can be disposed as a reaction of an atom with a diatomic molecule. This approximation is often used in the reactions of $X + CH_4$,[7–9,30–36] including the $O(^1D) + CH_4$ reaction,[7–9] which indicates the validity of this approximation. The potential energy surface is crucial for the reaction dynamics and there are many methods to obtain it, such as the double many-body expansion (DMBE) theory.[37,38] Gonzalez *et al*. put forward two triatomic PESs of the $O(^1D) + CH_4$ reaction[7,8] based on *ab initio* data. There is a barrier about 4.1 kcal/mol on the first PES, while the second one is barrierless. The second PES reproduces the experimental result of the rate constant accurately in contrast to the first PES.[8] So, the second PES is chosen in this work. Figure 1 shows the energy along the reaction path and the contour plots of the PES at the collinear configuration, which is the easiest way to react. There is no barrier in the reaction path, which suggests that the reaction does not present a threshold energy.

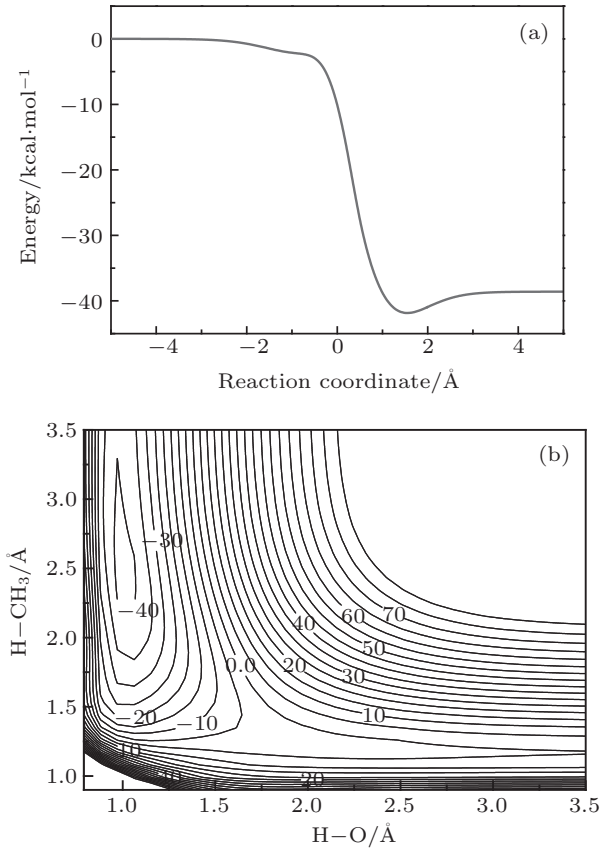


Fig. 1. (color online) (a) The energy along the reaction path for the collinear configuration. (b) Contour plots of the potential energy surface for the collinear configuration.

2.2. Product rotational polarization

The center of mass (CM) frame is used. The z axis is parallel to the reactant relative velocity $\boldsymbol{k}$ and the y axis is perpendicular to the xz plane containing reactant and product relative velocity vectors, $\boldsymbol{k}$ and $\boldsymbol{k}'$. The angle between $\boldsymbol{k}$ and $\boldsymbol{k}'$ is scattering angle θ, while θ_r and ϕ_r are the polar and azimuthal angles of the final rotational angular momentum $\boldsymbol{j}'$.[25,26] The fully correlated CM angular distribution is written as the sum[39]

$$P(\omega_t, \omega_r) = \sum_{kq} \frac{[k]}{4\pi} \frac{1}{\sigma} \frac{d\sigma}{d\omega_t} C_{kq}(\theta_r, \phi_r),$$

where $[k] = 2k+1$, $\frac{1}{\sigma}\frac{d\sigma}{d\omega_t}$ is the generalized polarization dependent differential cross sections (PDDCSs) and $C_{kq}(\theta_r, \phi_r)$ are the modified spherical harmonics. The differential cross section is given by

$$\frac{1}{\sigma}\frac{d\sigma_{00}}{d\omega_t} = P(\omega_t) = \frac{1}{4\pi}\sum_{k_1}[k_1] h_0^{k_1}(k_1, 0) P_{k_1}(\cos\theta_t).$$

The bipolar moment $h_0^{k_1}(k_1, 0)$ is evaluated using the expectation values of the Legendre moments of the differential cross section

$$h_0^{k_1}(k_1, 0) = \langle P_{k_1}(\cos\theta_t)\rangle.$$

The distribution $P(\theta_r)$ can be written as[39–42]

$$P(\theta_r) = \frac{1}{2}\sum(2k+1) a_0^{(k)} P_k(\cos\theta_r),$$

where

$$a_0^{(k)} = \int_0^{\pi} P(\theta_r) P_k(\cos\theta_r) \sin\theta_r \, d\theta_r = \langle P_k(\cos\theta_r)\rangle.$$

The coefficients $a_0^{(k)}$ are called the orientation (k is odd) or alignment (k is even) parameters. The $k = 2$ indicates the product rotational alignment[43]

$$a_0^2 = \langle P_2(\cos\theta_r)\rangle = \langle P_2(\boldsymbol{j}'\cdot\boldsymbol{k})\rangle = \frac{1}{2}\langle 3\cos^2\theta_r - 1\rangle.$$

Here, the average rotational alignment of the product is calculated only, as it has been measured in most experiments. The $P(\theta_r)$ is expanded up to k = 18, which shows a satisfactory convergence. The dihedral angle distribution function $P(\phi_r)$ describing the $\boldsymbol{k}$–$\boldsymbol{k}'$–$\boldsymbol{j}'$ correlation can be expanded in a Fourier series as

$$P(\phi_r) = \frac{1}{2\pi}\left(1 + \sum_{\text{even},n>2} a_n \cos n\phi_r + \sum_{\text{odd},n\geq 1} a_n \sin n\phi_r\right),$$

where $a_n = 2\langle\cos n\phi_r\rangle$ and $b_n = 2\langle\sin n\phi_r\rangle$. When $P(\phi_r)$ is expanded up to $n = 24$, it shows a satisfactory convergence.

2.3. Quasi-classical trajectory calculations

In this paper, we use the method of quasi-classical trajectory (QCT), which is often applied to study the product rotational polarization.[44–47] In the QCT calculations, Hamilton's classical equations are integrated numerically for motion. We choose the energy range from 2 kcal/mol to

20 kcal/mol, because the energy of most previous works is below 20.0 kcal/mol. The vibrational and rotational levels of the reactants are set as $v = 0$ and $j = 0$, respectively. Here, 100000 trajectories are sampled and the trajectories are initialized at an *A*–*BC* internuclear separation of 15 Å. To insure the numerical stability, the integration step size in the trajectories is set at 0.1 fs.

3. Results and discussion

In Fig. 2, the integral cross section for the title reaction is shown in the energy range from 2.0 kcal/mol to 20.0 kcal/mol. As the figure shows, there is no threshold energy as we predicted based on the feature of the PES; the value of the integral cross section (ICS) decreases with collision energy increasing. The total differential cross section, which defines the angular distribution of the product, contains much detailed information of the reactive scattering event. At different collision energies, 2.0 kcal/mol, 4.0 kcal/mol and 20.0 kcal/mol, the differential cross sections (DCSs) of the title reaction are shown in Fig. 3. The backward and the forward scatterings exist at the same time; the trend of both scatterings is more outstanding with collision energy increasing. As the figure shows, the forward scattering is more obvious than the backward scattering.

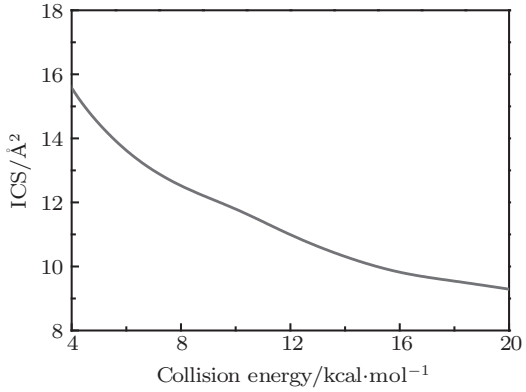


Fig. 2. Integral cross section of reaction $O(^1D) + CH_4 \rightarrow OH + CH_3$ in the energy range from 2.0 kcal/mol to 20.0 kcal/mol.

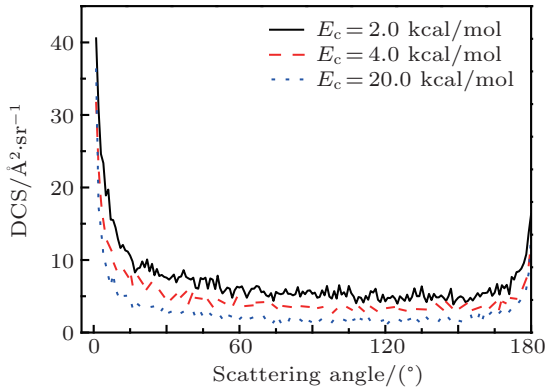


Fig. 3. (color online) A comparison of the total reactive DCSs at different E_c.

The distributions of $P(\theta_r)$ and $P(\phi_r)$ are plotted respectively in Figs. 4 and 5 to obtain a better graphical representation of the polarization of the product OH. In Fig. 4, it is clearly illustrated that the $P(\theta_r)$ distribution is maximum for θ_r close to 90° and symmetric with respect to $\theta_r = 90°$ due to the planar symmetry of the system. The result implies that in the product scattering frame, the $\boldsymbol{j}'$ is distributed with a cylindrical symmetry and the direction of $\boldsymbol{j}'$ is perpendicular preferentially to the $\boldsymbol{k}$ direction. With collision energy increasing, the peak of the $P(\theta_r)$ distribution becomes stronger; it means that the degree of the rotational alignment of the product OH increases with the collision energy increasing. The relationship between the dihedral angle distribution of the $\boldsymbol{k}$–$\boldsymbol{k}'$–$\boldsymbol{j}'$ and the collision energy is complicated. At different collision energies, the feature is obvious, as shown in Fig. 5. There are two peaks at $\phi_r = 90°$ and 270° in these $P(\phi_r)$ distributions. When collision energy $E_c = 2.0$ kcal/mol, the peak at $\phi_r = 90°$ is stronger than that at $\phi_r = 270°$. With the collision energy increasing, the peak at $\phi_r = 90°$ becomes weaker and the peak at $\phi_r = 270°$ becomes stronger. At $E_c = 8.0$ kcal/mol, the two peaks are roughly similar; at $E_c = 20.0$ kcal/mol, the advantage at $\phi_r = 270°$ is very obvious. So a conclusion can be obtained that the dominant angle in the $P(\phi_r)$ distribution changes from $\phi_r = 270°$ to $\phi_r = 90°$ with the increase of the collision energy.

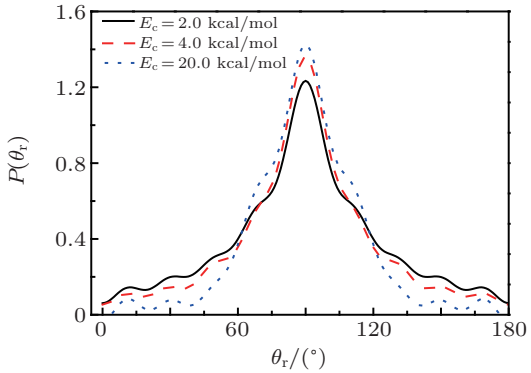


Fig. 4. (color online) The $P(\theta_r)$ reflecting the $\boldsymbol{k}$–$\boldsymbol{j}'$ correlation as a function of θ_r at different E_c.

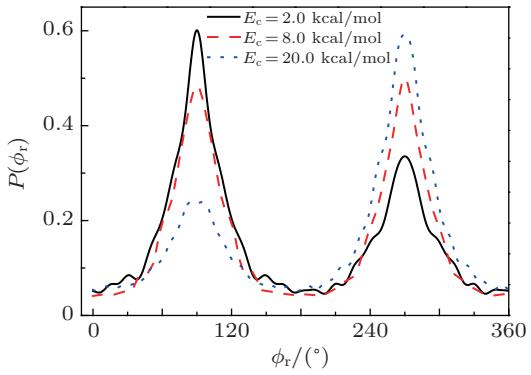


Fig. 5. (color online) Dihedral angle distributions $P(\phi_r)$ describing the relation of vectors $\boldsymbol{k}$–$\boldsymbol{k}'$–$\boldsymbol{j}'$ as a function of ϕ_r at different E_c.

In Fig. 6, the $P(\theta_r, \phi_r)$ distributions averaged over all scattering angles at three collision energies are plotted to get more information about the angular momentum polarization. When $E_c = 2.0$ kcal/mol, the peak at (90, 90) is stronger than that at (90, 270), which implies a preference for the right-handed OH rotation in planes parallel to the scattering plane. For $E_c = 8.0$ kcal/mol, the two peaks are similar, which means that the angular momentum vectors of the products are aligned along the y axis and not oriented. For $E_c = 20.0$ kcal/mol, the peak at (90, 270) is stronger than that at (90, 90), which implies a preference for the left-handed OH rotation in planes parallel to the scattering plane. So, with collision energy increasing, the dominant rotation of the product changes from the right-handed direction to the left-handed direction in planes parallel to the scattering plane.

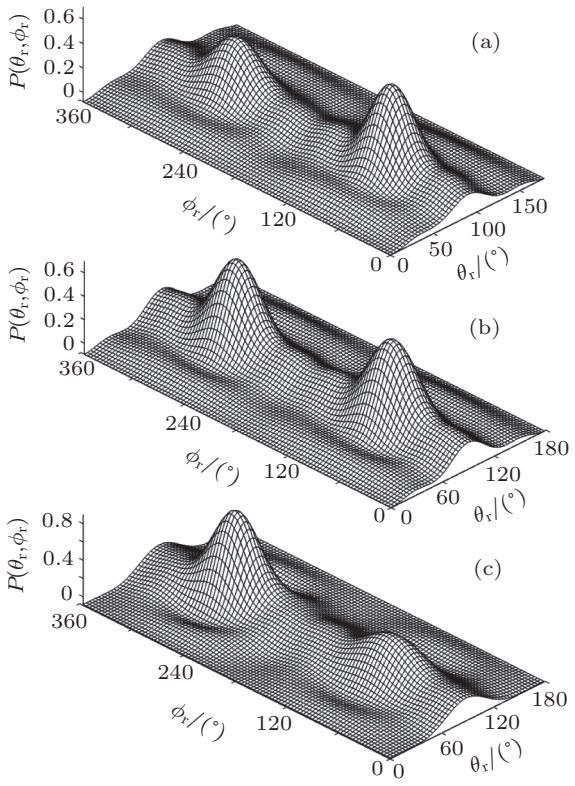


Fig. 6. Polar plots of $P(\theta_r, \phi_r)$ distributions averaged over all scattering angles at three collision energies of (a) 2.0 kcal/mol, (b) 8.0 kcal/mol and (c) 20.0 kcal/mol.

At the same collision energy, the mass combination is an important factor for reactive stereodynamics. The effect of the isotopic substitution can be embodied in two ways: mass factor and substituted position. The mass factor can be defined as $\cos^2\beta = m_A m_C/((m_A + m_B)(m_B + m_C))$ for the reaction $A + BC \rightarrow AB + C$; the rotational polarization may be very sensitive to the mass factor.[48] The collision energy of 8.0 kcal/mol is chosen to study the isotope effect in detail, where the B-positioned hydrogen atom is substituted by deuterium and tritium. The mass factors and integral cross sections are listed in Table 1.

Table 1. Mass factors of $O(^1D) + XCH_3 \rightarrow XO + CH_3$ (X = H, D, T) and the corresponding integral cross sections at 8.0 kcal/mol.

Reaction	$O + HCH_3$	$O + DCH_3$	$O + TCH_3$
$\cos^2\beta$	0.88	0.78	0.70
ICS/Å^2	12.5	8.85	7.69

The ICS is positively correlated with the mass factor, which implies the heavy B-positioned atom will reduce the reactivity. In Figs. 7 and 8, the $P(\theta_r)$ and $P(\phi_r)$ distributions are respectively shown to explore the isotope effect in the stereodynamics of the title reaction. In the $P(\theta_r)$ distribution, the peak of O+HCH_3 is stronger than the other two apparently, which indicates that the $P(\theta_r)$ distribution is sensitive to the mass factor from 0.88 to 0.78; the tendency of angular momentum vector $\boldsymbol{j}'$ paralleling to the relative velocity $\boldsymbol{k}$ is more obvious than that in the other two reactions. The $P(\theta_r)$ distributions of $O + DCH_3$ and $O + TCH_3$ are similar, which implies that the $P(\theta_r)$ distribution is not sensitive to the change of mass factor from 0.78 to 0.70. In the distribution of $P(\phi_r)$, with the mass factor decreasing, the peaks at $\phi_r = 90°$ and $\phi_r = 270°$ become weaker. For the reaction of $O + D/TCH_3$, the peak at $\phi_r = 270°$ is prominent, which indicates that more products tend to rotate in the negative direction of the y axis in planes parallel to the scattering plane. In summary, the decrease of the mass factor, i.e., heavy of the B-positioned atom, weakens the polarization degree of the rotational angular momentum vectors of the products.

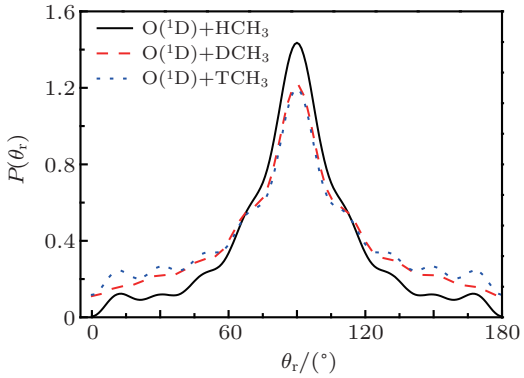


Fig. 7. (color online) A comparison of $P(\theta_r)$ distributions of the three reactions, $O(^1D) + XCH_3 \rightarrow XO + CH_3$ (X = H, D, T), at E_c = 8.0 kcal/mol.

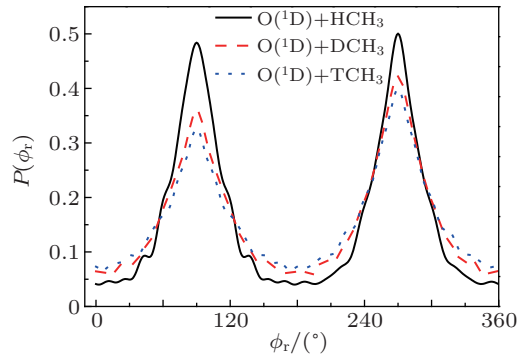


Fig. 8. (color online) A comparison of $P(\phi_r)$ distributions of the three reactions, $O(^1D) + XCH_3 \rightarrow XO + CH_3$ (X = H, D, T), at E_c = 8.0 kcal/mol.

4. Conclusion

In this work, we carried out a quasiclassical trajectory dynamic study on the reaction $O(^1D)+CH_4 \rightarrow OH+CH_3$ using the potential energy surface obtained by Gonzalez *et al*. The integral cross sections, total differential cross sections and product rotational angular momentum polarization have been calculated to explore the stereodynamics of the reaction. The ICS has a negative correlation with the collision energy. In the reaction, the backward and forward scatterings exist at the same time, which gets more obvious with the increase of the collision energy. With the collision energy increasing, the dominant place in the $P(\theta_r, \phi_r)$ distribution changes from (90, 90) to (90, 270) gradually; at $E_c = 8.0$ kcal/mol, the peak heights at both places have a similar value. In the study on the isotopic effect, we come to the conclusion that a heavy *B*-positioned atom weakens the polarization degree of the rotational angular momentum vectors of the product.

References

[1] Blitz M A, Dillon T J, Heard D E, Pilling M J and Trought I D 2004 *Phys. Chem. Chem. Phys.* **6** 2162
[2] Lin J J, Lee Y T and Yang X 1998 *J. Chem. Phys.* **109** 2975
[3] Lin J J, Harich S, Lee Y T and Yang X 1999 *J. Chem. Phys.* **110** 10821
[4] Lin J J, Shu J, Lee Y T and Yang X 2000 *J. Chem. Phys.* **113** 5287
[5] Miller C C, van Zee R D and Stephenson J C 2001 *J. Chem. Phys.* **114** 1214
[6] Shuai Q, Pan H L, Yang J Y, Zhang D, Jiang B, Dai D X and Yang X M 2012 *J. Phys. Chem. Lett.* **3** 1310
[7] Gonzalez M, Hernando J, Banos I and Sayos R 1999 *J. Chem. Phys.* **111** 8913
[8] Gonzalez M, Hernando J, Puyuelo M P and Sayos R 2000 *J. Chem. Phys.* **113** 6748
[9] Gonzalez M, Puyuelo M P, Hernando J, Sayos R, Enriquez P A, Guallar J and Banos I 2000 *J. Phys. Chem. A* **104** 521
[10] Chang A H H and Lin S H 2004 *Chem. Phys. Lett.* **384** 229
[11] Chang A H H and Lin S H 2002 *Chem. Phys. Lett.* **363** 175
[12] Yu H G and Muckerman J T 2004 *J. Phys. Chem. A* **108** 8615
[13] Kohguchi H, Ogi Y and Suzuki T 2011 *Phys. Chem. Chem. Phys.* **13** 8371
[14] Kohguchi H, Ogi Y and Suzuki T 2008 *Phys. Chem. Chem. Phys.* **10** 7222
[15] Yang X M 2006 *Phys. Chem. Chem. Phys.* **8** 205
[16] Hancock G, Morrison M and Saunders M 2005 *J. Photoch. Photobio. A* **176** 191
[17] Chen H B, Thweatt W D, Wang J J, Glass G P and Curl R F 2005 *J. Phys. Chem. A* **109** 2207
[18] Hernando J, Millan J, Sayos R and Gonzalez M 2003 *J. Chem. Phys.* **119** 9504
[19] Sayos R, Hernando J, Puyuelo M P, Enriquez P A and Gonzalez M 2002 *Phys. Chem. Chem. Phys.* **4** 288
[20] Saueressig G, Crowley J N, Bergamaschi P, Bruhl C, Brenninkmeijer C A M and Fischer H 2001 *J. Geophys. Res-Atmos.* **106** 23127
[21] Ogi Y, Kohguchi H and Suzuki T 2013 *Phys. Chem. Chem. Phys.* **15** 12946
[22] Ausfelder F, Hippler H and Striebel F 2000 *Z. Phys. Chem.* **214** 403
[23] Wada S and Obi K 1998 *J. Phys. Chem. A* **102** 3481
[24] Shuai Q, Pan H, Yang J, Zhang D, Jiang B, Dai D and Yang X 2012 *J. Chem. Phys.* **137** 224301
[25] Barnwell J D, Loeser J G and Herschbach D R 1983 *J. Phys. Chem.* **87** 2781
[26] Mcclelland G M and Herschbach D R 1979 *J. Phys. Chem.* **83** 1445
[27] Case D A and Herschbach D R 1975 *Mol. Phys.* **30** 1537
[28] Fano U and Macek J H 1973 *Rev. Mod. Phys.* **45** 553
[29] Orrewing A J and Zare R N 1994 *Annu. Rev. Phys. Chem.* **45** 315
[30] Troya D, Millan J, Banos I and Gonzalez M 2004 *J. Chem. Phys.* **120** 5181
[31] Liu Y F, Gao Y L, Zhai H S, Shi D H and Sun J F 2009 *Int. J. Mol. Sci.* **10** 2146
[32] Martinez R, Enriquez P A, Puyuelo M P and Gonzalez M 2012 *J. Phys. Chem. A* **116** 5026
[33] Gonzalez M, Hernando J, Millan J and Sayos R 1999 *J. Chem. Phys.* **110** 7326
[34] Troya D, Millan J, Banos I and Gonzalez M 2002 *J. Chem. Phys.* **117** 5730
[35] Gauss A 1976 *J. Chem. Phys.* **65** 4365
[36] Cheng D H, Yuan J C, Yang T G and Chen M D 2013 *Chin. Phys. B* **22** 068202
[37] Li Y Q, Yuan J C, Chen M D, Ma F C and Sun M T 2013 *J. Comput. Chem.* **34** 1686
[38] Li Y Q, Song Y Z, Song P, Li Y Z, Ding Y, Sun M T and Ma F C 2012 *J. Chem. Phys.* **136** 194705
[39] Shaferray N E, Orrewing A J and Zare R N 1995 *J. Phys. Chem.* **99** 7591
[40] Wang M L, Han K L and He G Z 1998 *J. Chem. Phys.* **109** 5446
[41] Wang M L, Han K L and He G Z 1998 *J. Phys. Chem. A* **102** 10204
[42] Brouard M, Lambert H M, Rayner S P and Simons J P 1996 *Mol. Phys.* **89** 403
[43] Han K L, He G Z and Lou N Q 1996 *J. Chem. Phys.* **105** 8699
[44] Duan L H, Zhang W Q, Xu X S, Cong S L and Chen M D 2009 *Mol. Phys.* **107** 2579
[45] Yang T G, Yuan J C, Cheng D H and Chen M D 2013 *Commn. Comput. Chem.* **1** 15
[46] Zhang W Q, Cong S L, Zhang C H, Xu X S and Chen M D 2009 *J. Phys. Chem. A* **113** 4192
[47] Zhang W Q and Chen M D 2009 *J. Theor. Comput. Chem.* **8** 1131
[48] Zhang W Q, Li Y Z, Xu X S and Chen M D 2010 *Chem. Phys.* **367** 115